Bioresource Technology 111 (2012) 185–190

Contents lists available at SciVerse ScienceDirect

Bioresource Technology

journal homepage: www.elsevier.com/locate/biortech

Activated carbons from KOH-activation of argan (*Argania spinosa*) seed shells as supercapacitor electrodes

Abdelhakim Elmouwahidi [1], Zulamita Zapata-Benabithe [2], Francisco Carrasco-Marín, Carlos Moreno-Castilla *

Departamento de Química Inorgánica, Universidad de Granada, 18071 Granada, Spain

ARTICLE INFO

Article history:
Received 20 December 2011
Received in revised form 1 February 2012
Accepted 2 February 2012
Available online 14 February 2012

Keywords:
Energy storage
Supercapacitors
Activated carbons
Argan seed shells
KOH-activation

ABSTRACT

Activated carbons were prepared by KOH-activation of argan seed shells (ASS). The activated carbon with the largest surface area and most developed porosity was superficially treated to introduce oxygen and nitrogen functionalities. Activated carbons with a surface area of around 2100 m^2/g were obtained. Electrochemical measurements were carried out with a three-electrode cell using 1 M H_2SO_4 as electrolyte and Ag/AgCl as reference electrode. The O-rich activated carbon showed the lowest capacitance (259 F/g at 125 mA/g) and the lowest capacity retention (52% at 1 A/g), due to surface carboxyl groups hindering electrolyte diffusion into the pores. Conversely, the N-rich activated carbon showed the highest capacitance (355 F/g at 125 mA/g) with the highest retention (93% at 1 A/g), due to its well-developed micro-mesoporosity and the pseudocapacitance effects of N functionalities. This capacitance performance was among the highest reported for other activated carbons from a large variety of biomass precursors.

1. Introduction

Electrochemical double-layer capacitors (EDLCs) or supercapacitors are energy storage devices that store the electrical energy in an electrochemical double-layer formed at the interface between the charged surface of the electrode and the electrolyte solution (Qu and Shi, 1998; Conway, 1999). Porous carbon materials are widely used as electrodes owing to their high surface area, well-developed pore-size distribution, which can be adapted to the size of the electrolyte ions, high conductivity, and good physicochemical stability. In addition, carbon surfaces can be decorated with electrochemically active surface functionalities that modify the double-layer capacitance (Pandolfo and Hollenkamp, 2006; Frackowiak, 2007; Zhang and Zhao, 2009).

Activated carbons are porous carbon materials of great interest for utilization as supercapacitor electrodes because they can be readily prepared from cheap biomass residues and wastes. Thus, activated carbons have been prepared from rice husk (Guo et al., 2003), firwood and pistachio shells (Wu et al., 2004, 2005), bamboo (Kim et al., 2006), banana fibers (Subramanian et al., 2007), waste coffee beans (Rufford et al., 2008), corn grains (Balathanigaimani et al., 2008), cassava peel waste (Ismanto et al., 2010), sugar cane bagasse (Rufford et al., 2010), and sunflower seed shells (Li et al., 2011).

The argan tree (*Argania spinosa*) is an endemic species in the Southwestern region of Morocco, and its seeds are used to produce oil of value for culinary and cosmetic uses. Argan oil processing produces large quantities of biomass residues (ASS) that are mainly used for heating purposes.

The objective of this study was to investigate the applicability of activated carbons derived from ASS as supercapacitor electrodes. Activated carbons were prepared by KOH-activation following a method previously used to obtain activated carbons from olive-mill waste water (Moreno-Castilla et al., 2001) and olive stones (Ubago-Pérez et al., 2006). The activated carbon with the best surface characteristics was further superficially treated to introduce oxygen and nitrogen functionalities. The prepared activated carbons were characterized to determine their pore texture, surface chemistry, and electrochemical characteristics. Results were compared with published findings for activated carbons prepared from other biomass residues and wastes.

2. Experimental

2.1. Preparation of activated carbon

Three activated carbons were prepared from ASS. Ground ASS with a particle size between 2 and 3 mm was carbonized under N_2 flow (300 cm^3/min) at 500 °C for 3 h and designated sample C. Portions of ASS and sample C were chemically activated with KOH. For this purpose, both samples were mixed with a

* Corresponding author. Tel.: +34 958 243323; fax: +34 958 248563.
E-mail address: cmoreno@ugr.es (C. Moreno-Castilla).
[1] Address: Departament de Chimie, Université Caddi-Ayyad, Marrakech, Morocco.
[2] Address: Facultad de Ingeniería Química, Universidad Pontificia Bolivariana, 050031 Medellín, Colombia.

0960-8524/$ - see front matter © 2012 Elsevier Ltd. All rights reserved.
doi:10.1016/j.biortech.2012.02.010

concentrated KOH solution to obtain two slurries with a KOH/sample weight ratio of 4. The slurries were heated at 60 °C for 12 h and then at 110 °C to dryness. Next, samples were pyrolized under N_2 flow (300 cm^3/min) at 300 °C for 2 h and then at 800 °C for 3 h at a heating rate of 10 °C/min. The activated carbons prepared from ASS and C were designated samples AK and CK, respectively. A third activated carbon, AP, was prepared by physically mixing ASS and solid KOH at a KOH/ASS weight ratio of 4. Prepared activated carbons were washed with 0.1 M HCl and then with distilled water until chloride ions were no longer detected in the washing water by using a silver nitrate solution.

Portions of activated carbon AK were further superficially modified by treatment with ammonium peroxydisulfate (sample AKO) and melamine (sample AKN) to introduce surface oxygen and nitrogen functionalities, respectively. Oxidation with ammonium peroxydisulfate was performed as reported by Moreno-Castilla et al. (1995). Sample AKN was prepared by mixing 1 g of AK with 70 mg of melamine dissolved in 40 mL ethanol. After stirring this slurry, the solvent was slowly evaporated and the remaining residue was heat-treated at 750 °C for 1 h under N_2 flow (60 cm^3/min). This procedure was carried out according to Seredych et al. (2008) with minor modifications. The preparation conditions and designations of these activated carbons are shown in Table 1.

2.2. Characterization of activated carbons

Activated carbons were characterized by N_2 and CO_2 adsorption at −196 and 0 °C using Autosorb 1 from Quantachrome after outgassing the samples overnight at 110 °C under high vacuum (10^{-6} mbar). The BET equation was applied to N_2 adsorption isotherms to obtain the apparent BET surface area, S_{BET}, considering the molecular area of N_2 at −196 °C to be 0.162 nm^2 (Rodríguez-Reinoso and Linares-Solano, 1989). The Dubinin–Radushkevich (DR) equation was applied to the N_2 and CO_2 isotherms to obtain the micropore volume accessible to these adsorptives, W_0, and the mean micropore width, L_0. The total pore volume was obtained from the amount of N_2 adsorbed at $p/p_0 = 0.95$, $V_{0.95}$, and the mesopore volume, V_{meso}, from the difference between $V_{0.95}$ and $W_0(N_2)$. The pore size distribution (PSD) was determined by applying Quenched Solid Density Functional Theory (QSDFT) to the N_2 adsorption isotherms, assuming slit-shaped pores.

Immersion enthalpies into benzene, ΔH_{benz}, and water, ΔH_{water}, were determined with a C80-D Setaram calorimeter after outgassing the samples overnight under a dynamic vacuum of 10^{-6} mbar at 120 °C. Measurements were carried out at 30 °C and at least twice for each sample. ΔH_{benz} was used to determine the surface area of the activated carbons, S_{benz}, considering the immersion enthalpy into benzene of a non-porous graphitized carbon black to be 0.114 J/m^2 (Denoyel et al., 1993). The hydrophobicity of samples was determined from Eq. (1)

$$\text{Hydrophobicity} = 1 - (\Delta H_{water}/\Delta H_{benz}) \quad (1)$$

Temperature programmed desorption (TPD) was performed by heating samples to 1000 °C at 10 °C/min and analyzing the CO and CO_2 evolved by means of a model Prisma mass spectrometer from Pfeiffer (Germany). The total oxygen content, O_{TPD}, was calculated from the amount of CO and CO_2 evolved. The total N content, N_{CHN}, was determined by elemental analysis.

X-ray photoelectron spectroscopy (XPS) was performed using an Escalab 200R system (VG Scientific Co.) equipped with MgK_α X-ray source ($h\gamma$ = 1253.6 eV) and hemispherical electron analyzer. Survey and multi-region spectra were recorded at C_{1s}, O_{1s}, and N_{1s} photoelectron peaks. Each spectral region of photoelectron interest was scanned several times to obtain good signal-to-noise ratios. The C_{1s} peak at 284.6 eV was used as internal standard.

2.3. Electrochemical measurements

Electrochemical measurements were carried out in a Biologic multichannel potentiostat at room temperature using 1 M H_2SO_4 as electrolyte, a typical three-electrode cell with Ag/AgCl as reference electrode, and Pt wire as counter electrode. The working electrode was graphite paper on which a homogeneous mixture of finely ground activated carbon, acetylene black, and binder (polytetrafluoroethylene, PTFE) at a mass ratio of 80:10:10 was pasted.

Cyclic voltammograms were obtained at different scan rates, and the gravimetric capacitance, C_{CV} (F/g), was calculated from these curves by Eq. (2)

$$C_{CV} = \frac{\Sigma|I|\Delta t}{2m\Delta V} \quad (2)$$

where $\Sigma|I|\Delta t$ is the area of the current (A) against time (s) curve, m the mass of active material in the electrode (g), and ΔV the potential window (V). Chronopotentiograms were performed at a current loading between 125 and 1000 mA/g in a potential interval of 0–0.75 V. The gravimetric capacitance from these measurements, C_{CP} (F/g), was obtained by Eq. (3).

$$C_{CP} = \frac{I_d \Delta t}{m\Delta V} \quad (3)$$

where I_d is the discharge current (A) in the potential range between 0.3 and 0.1 V, Δt the discharge time (s), and ΔV the potential interval (V).

3. Results and discussion

Fig. 1 depicts N_2 adsorption isotherms of the activated carbons AP, CK, and AK and of the superficially modified activated carbons AKO and AKN. They are typical type I microporous carbons according to IUPAC classification, but the shape of the isotherms in sample AK and its derivatives AKO and AKN showed a wide knee indicative of a micro-mesopore structure. Fig. 2 depicts the pore size distribution obtained by applying the QSDFT method to these isotherms, and Table 2 exhibits the surface area and porosity values.

All samples showed $W_0(N_2) > W_0(CO_2)$, indicating an absence of constrictions at micropore entrances and hence complete accessibility to N_2 molecules at −196 °C (Rodríguez-Reinoso and Linares-Solano, 1989). S_{BET} and S_{benz} surface area values were similar, because the minimal dimensions of N_2 (0.36 nm) and

Table 1
Preparation conditions of activated carbons from argan seed shell (ASS).

Sample	Raw material	KOH/raw material weight ratio = 4	Pyrolysis temperature (°C)–time (h)	Surface treatment
C	ASS	–	500–2	–
CK	C	Aqueous slurry	300–2; 800-3	–
AK	ASS	Aqueous slurry	300–2; 800-3	–
AP	ASS	Physical mixture	300–2; 800-3	–
AKO	AK	–	–	$(NH_4)_2S_2O_8$
AKN	AK	–	750–5	Melamine

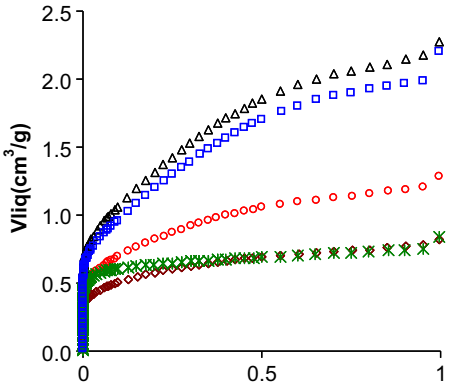

Fig. 1. N_2 adsorption isotherms at −196 °C on activated carbons: ◇, AP; ✳, CK; △, AK; ○, AKO; □, AKN.

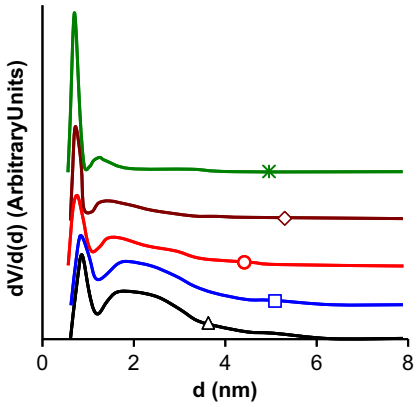

Fig. 2. Pore size distribution of activated carbons by application of QSDFT method to N_2 adsorption isotherms at −196 °C. ◇, AP; ✳, CK; △, AK; ○, AKO; □, AKN.

Table 2
Surface area and porosity of the activated carbons.

	C	AP	CK	AK	AKO	AKN
Surface area						
S_{BET} (m^2/g)	21	1279	1430	2132	1654	2062
$-\Delta H_{benz}$ (J/g)	nd	143.7	154.5	234.3	186.2	233.9
S_{benz} (m^2/g)	nd	1261	1355	2055	1633	2052
S_{BET}/S_{benz}	nd	1.01	1.06	1.04	1.01	1.00
Porosity						
$W_0(N_2)$ (cm^3/g)	–	0.47	0.58	0.96	0.62	0.95
$W_0(CO_2)$ (cm^3/g)	–	0.39	0.54	0.44	0.40	0.37
$L_0(N_2)$ (nm)	–	1.2	0.8	1.4	1.3	1.4
$L_0(CO_2)$ (nm)	–	0.8	0.8	0.8	0.8	0.9
$V_{0.95}$ (cm^3/g)	–	0.78	0.76	2.18	1.20	1.99
V_{meso} (cm^3/g)	–	0.31	0.10	1.22	0.58	1.04

nd: Not determined.

benzene (0.37 nm) are almost identical (Villar-Rodil et al., 2002), and the micropore width allowed the accommodation of one N_2 monolayer on each micropore wall. The three activated carbons (AP, CK, AK) showed a bimodal PSD (Fig. 2). This PSD was essentially within the micropore range in the case of CK, which had the lowest mesopore volume. However, The PSD of sample AK was in the micro-mesopore range up to a width of a few nanometers in the lower range of mesopores.

Among these activated carbons, the largest surface area and micro- and mesopore volumes were found in sample AK, prepared by activation of ASS previously impregnated with an aqueous KOH solution. This preparation yielded a better distribution of the activating agent within the precursor particles in comparison to the physical mixture of solid KOH and precursor (activated carbon AP). Use of the non-carbonized precursor to obtain AK rather than the carbonized precursor to obtain CK created a more intensive KOH interaction during activation, producing a larger surface area and higher pore volumes. Thus, $W_0(N_2)$ and V_{meso} increased from 0.58 and 0.10 cm^3/g in CK to 0.96 and 1.22 cm^3/g, respectively, in AK. Similar observations were reported for the KOH-activation of non-carbonized and carbonized olive stones (Ubago-Pérez et al., 2006) and coals (Lillo-Ródenas et al., 2003).

The oxidation of AK to obtain AKO, which fixed a large amount of oxygen on the surface (Table 3), also reduced the S_{BET} and micro- and mesopore volumes by partially destroying micro and mesopore walls (Moreno-Castilla et al., 1995, 1997). Melamine treatment of AK to obtain AKN was less drastic and only slightly reduced V_{meso}, as previously reported for melamine-treated activated carbons (Seredych et al., 2008).

The microporosity of the samples with $L_0(N_2)$ between 0.8 and 1.4 nm, would be fully accessible to the hydronium ions, 0.36–0.42 nm (Eliad et al., 2001), and hydrated bisulfate ions, 0.53 nm (Endo et al., 2001; Moreno-Castilla et al., in press), produced by dissociation of the electrolyte (1 M H_2SO_4).

The surface chemistry of the activated carbons is summarized in Tables 3 and 4. The three activated carbons AP, CP and AK showed similar ash, oxygen, and nitrogen contents, CO/CO_2 ratio, and hydrophobicity. The oxygen content of sample AKO was very high (20%) and was homogeneously distributed between the internal and the external surface of the sample, as shown by the similarity of the O_{TPD} and O_{XPS} values. The CO/CO_2 ratio was lower in AKO than in AK because the oxidation mainly increased the amount of CO_2-evolving groups such as carboxyl acid groups, which are known to increase during peroxydisulfate treatment (Moreno-Castilla et al., 1995, 1997). The hydrophobicity (Table 3) markedly decreased as a consequence of the fixation of oxygen functionalities with large polarity, e.g., carboxyl groups. As shown in Table 4, both AK and AKO samples had a higher concentration of surface

Table 3
Ash content, amounts of CO and CO_2 evolved up to 1000 °C, total and surface O and N concentrations, immersion enthalpies into water and benzene, and hydrophobicity of the activated carbons.

	AP	CK	AK	AKO	AKN
Ash (%)	4.6	4.1	4.4	3.1	4.2
CO (μmol/g)	2.92	2.31	2.97	6.48	1.52
CO_2 (μmol/g)	0.53	0.40	0.54	3.01	0.11
CO/CO_2	5.51	5.78	5.50	2.15	13.8
O_{TPD} (wt.%)	6.4	5.0	6.5	20.0	2.8
O_{XPS} (wt.%)	nd	nd	7.6	20.3	4.1
N_{CHN} (wt.%)	0.8	0.9	0.8	0.5	1.6
N_{XPS} (wt.%)	nd	nd	0.9	0.6	2.0
$-\Delta H_{water}$ (J/g)	84.1	81.4	110.1	224.4	108.8
Hydrophobicity	0.41	0.43	0.53	-0.21	0.53

nd: Not determined.

Table 4
Relative surface concentrations (%) of O and N functionalities from the deconvolution of O_{1s} and N_{1s} XP spectra.

Binding energy (eV)	Functionality	AK	AKO	AKN
O_{1s}				
531.4–531.8	C=O bonds	33	38	44
533.0–533.3	C–OH bonds	56	62	56
534.7	H_2O	11	–	–
N_{1s}				
398	N-6	20	32	43
400	N-5	41	48	39
401	N-Q	39	20	18

functionalities with single C–O bonds (e.g., carboxyl and phenol groups) than with double C=O bonds (e.g., carboxyl and quinone groups).

Melamine treatment of AK to obtain AKN increased the N content, which was distributed across pyridinic (N-6), pyrrolic, and/or pyridonic (N-5) and quaternary-N (N-Q) groups (Pels et al., 1995). The treatment greatly increased the amount of N-6 functionalities and reduced the amount of N-Q functionalities. Both O_{TPD} and O_{XPS} were decreased, mainly due to the loss of CO_2-evolving groups. The hydrophobicity of the activated carbon was not changed by the melamine treatment.

Fig. 3 depicts typical cyclic voltammograms at 0.5 mV/s. The three activated carbons AP, CK and AK showed a symmetric and quasi-rectangular shape profile typical of ideal EDLCs, with very small humps attributed to pseudofaradaic redox reactions related to the surface functionalities of the materials (Kinoshita, 1988). C_{CV} values at 0.5 mV/s are compiled in Table 5; AK had the highest value among the activated carbons because it had the largest microporosity and surface area.

The cyclic voltammogram of AKO (Fig. 3) shows that the capacitance increased with increases in the potential across the entire range of the potential window, indicating a slow charging process due to pore resistance. The presence of surface quinone groups increases the capacitance of oxidized activated carbons by introducing pseudocapacitance effects; however, oxidation also fixes other surface oxygen complexes such as carboxyl groups which, due to their high polarity, bind water molecules that hinder and retard electrolyte diffusion into the microporosity, thereby increasing its ohmic resistance (Guo et al., 2003).

Hence, the increase in capacitance due to the presence of quinone groups can be offset by an increased inner resistance due to the presence of carboxyl groups. Table 5 shows a large decrease of C_{CV} from 321 F/g in sample AK to 228 F/g in sample AKO. This can be attributed to the large amount of CO_2-evolving groups (e.g., carboxyl acids) present in the AKO sample, producing a major reduction in its hydrophobicity.

Sample AKN also showed a quasi-rectangular cyclic voltammogram. The C_{CV} value obtained at 0.5 mV/s (Table 5) was the highest

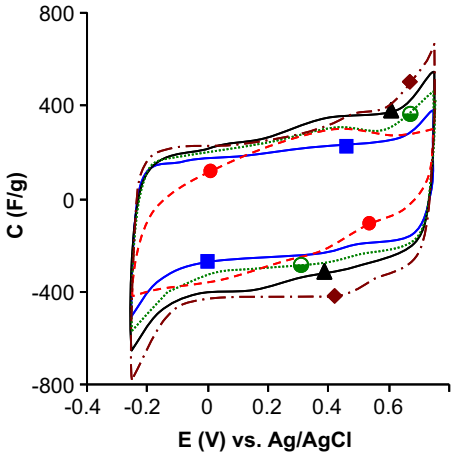

Fig. 3. Cyclic voltammograms of activated carbons using a three-electrode cell in 1 M H_2SO_4 at 0.5 mV/s. ■, AP; ◒, CK; ▲, AK; ●, AKO; ◆, AKN.

Table 5
Gravimetric capacitances: C_{CV} at 0.5 mV/s and C_{CP} at 125 mA/g and 1 A/g, and C_{CP} retention.

Sample	C_{CV} (F/g)	C_{CP} (F/g) (at 125 mA/g)	C_{CP} (F/g) (at 1 A/g)	C_{CP} retention (%)
AP	234	272	175	64
CK	277	269	242	90
AK	321	325	291	90
AKO	228	259	135	52
AKN	358	355	329	93

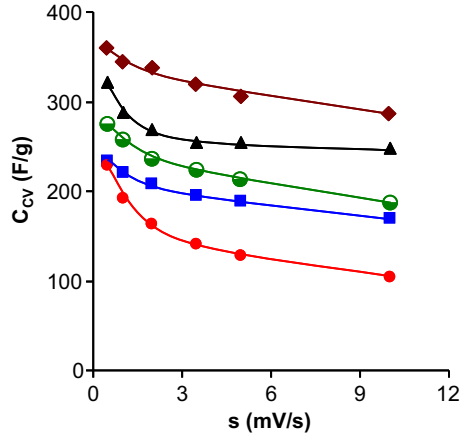

Fig. 4. Variation in C_{CV} gravimetric capacitance with scan rate. ■, AP; ◒, CK; ▲, AK; ●, AKO; ◆, AKN.

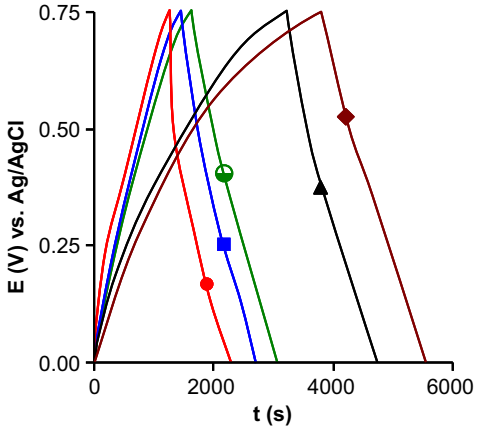

Fig. 5. Chronopotentiograms of activated carbons using a three-electrode cell in 1 M H_2SO_4 at 125 mA/g. ■, AP; ◒, CK; ▲, AK; ●, AKO; ◆, AKN.

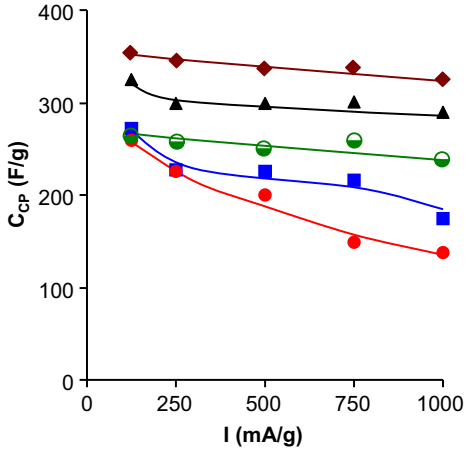

Fig. 6. Influence of current loading on C_{CP} gravimetric capacitance of activated carbons. ■, AP; ◒, CK; ▲, AK; ●, AKO; ◆, AKN.

Table 6
Maximum capacitances of activated carbons from biomass precursors. Capacitances are the three-electrode equivalents for a single electrode.

Biomass precursor	Activation method	S_{BET} (m^2/g)	Maximum capacitance (F/g)	Capacitance measurement at	Electrolyte	Reference
Rice husk	NaOH	1886	210	0.2 mA/g	3 M KCl	Guo et al. (2003)
Firwood	H_2O	1131	140	25 mV/s	0.5 M H_2SO_4	Wu et al. (2004)
Pistachio shell	KOH	1096	120	10 mV/s	0.5 M H_2SO_4	Wu et al. (2005)
Firwood	KOH	1064	180	10 mV/s	0.5 M H_2SO_4	Wu et al. (2005)
Bamboo	KOH	1251	260[a]	1 mA/cm^2	30 wt.% H_2SO_4	Kim et al. (2006)
Banana fibers	$ZnCl_2$	1097	74	500 mA/g	1 M Na_2SO_4	Subramanian et al. (2007)
Corn grains	KOH	3199	257	1 mA/cm^2	6 M KOH	Balathanigaimani et al. (2008)
Waste coffee beans	$ZnCl_2$	1019	368	50 mA/g	1 M H_2SO_4	Rufford et al. (2008)
Sugar cane bagasse	$ZnCl_2$	1788	300	250 mA/g	1 M H_2SO_4	Rufford et al. (2010)
Cassava peel waste	KOH	1352	153	–	0.5 M H_2SO_4	Ismanto et al. (2010)
Sunflower seed shell	KOH	2509	311	250 mA/g	30 wt.% KOH	Li et al. (2011)
Argan seed shell	KOH/melamine	2062	355	125 mA/g	1 M H_2SO_4	This work

[a] The two-electrode gravimetric capacitance value published was converted to the three-electrode equivalent for a single electrode.

obtained in any sample. It has been reported that surface N functionalities (e.g., pyridinic, pyrrolic and pyridonic nitrogen) are electrochemically active because they are electron-rich (Frackowiak, 2007; Rufford et al., 2008). Protons can therefore be attracted to the electrode surface, giving rise to pseudocapacitive interactions (Hulicova et al., 2005). The surface concentration of pyridinic nitrogen was higher in sample AKN than in sample AK, which may explain the higher capacitance of the former.

The gravimetric capacitance of the samples is plotted against the scan rate in Fig. 4. C_{CV} decreased with increased scan rate because the formation of the electrochemical double-layer within the micropores is slower and less complete in comparison to the rate of variation in potential. Sample AKO showed the highest loss of capacitance with increased scan rate, attributable to the presence of highly polar surface oxygen groups that would hinder diffusion of the electrolyte into the micropores.

Typical chronopotentiograms are depicted in Fig. 5 at a current load of 125 mA/g. C_{CP} values at 125 mA/g and 1 A/g are compiled in Table 5. C_{CP} values at the lowest current load were close to C_{CV} values at 0.5 mV/s. The variation in C_{CP} with increasing current load is depicted in Fig. 6. Sample AKN showed the highest C_{CP} value, 355 F/g, at the current load of 125 mA/g, which is excellent for an activated carbon (Pandolfo and Hollenkamp, 2006; Rufford et al., 2010). It also had the highest capacitance retention (93%) at the higher current load of 1 A/g.

AKN and AK had similar surface areas and micropore textures, and the higher gravimetric capacitance of the former is related to the larger amount of pyridinic-N and therefore pseudocapacitance effects. Both samples had the same capacitance retention at high current load (Table 5) because of the similarity of their mesopore textures. Small mesopores influence the capacitance retention at high current loads, and are known to facilitate transport of ions through the carbon porosity at fast charge–discharge rates (Rufford et al., 2010; Zhao et al., 2010).

Sample AKO showed the lowest C_{CP} at 125 mA/g and the lowest capacity retention (52%) at 1 A/g, because the presence of surface carboxyl groups hampers electrolyte diffusion into the highly polar pores.

The performances as supercapacitor electrodes of the activated carbons prepared from ASS by KOH-activation, especially those of samples AK and AKN, was among the best reported for activated carbons prepared from a wide variety of biomass precursors (Table 6). ASS can therefore be successfully used to prepare porous activated carbons by KOH-activation for EDLC applications. This is attributable to the development of a microporous network that is accessible to the electrolyte ions and is interconnected with small mesopores. Their capacitance performance is further enhanced by the ease with which N-functionalities can be introduced.

4. Conclusions

The electrochemical performance of activated carbons prepared by KOH-activation of ASS was compared with published reports on other activated carbons, demonstrating that ASS is an excellent biomass precursor for the preparation of porous activated carbons for supercapacitor applications. The highest capacitance obtained was 355 F/g at 125 mA/g with a 93% retention capacitance at 1 A/g, attributable to the large surface area, appropriate and well-developed micro-mesopore texture, and N content of the activated carbon.

Acknowledgements

The authors are grateful to AECID, Ministerio de Asuntos Exteriores y Cooperación, Spain for financial support through Project A/024015/09. ZZB acknowledges a pre-doctoral fellowship from COLCIENCIAS, Colombia.

References

Balathanigaimani, M.S., Shim, W.G., Lee, M.J., Kim, C., Lee, J.W., Moon, H., 2008. Highly porous electrodes from novel corn grains-based activated carbons for electrical double layer capacitors. Electrochem. Commun. 10, 868–871.
Conway, B.E., 1999. Electrochemical supercapacitors. Scientific Fundamentals and Technological Applications. Kluwer Academic, New York.
Denoyel, R., Fernández-Colinas, J., Grillet, Y., Rouquerol, J., 1993. Assessment of the surface area and microporosity of activated charcoals from immersion calorimetry and nitrogen adsorption data. Langmuir 9, 515–518.
Eliad, L., Salitra, G., Soffer, A., Aurbach, D., 2001. Ion sieving effects in the electrical double layer of porous carbon electrodes: estimating effective ion size in electrolytic solutions. J. Phys. Chem. B 105, 6880–6887.
Endo, M., Maeda, T., Takeda, T., Kim, Y.J., Koshiba, K., Hara, H., Dresselhauss, M., 2001. Capacitance and pore-size distribution in aqueous and nonaqueous electrolytes using various activated carbon electrodes. J. Electrochem. Soc. 148, A910–A914.
Frackowiak, E., 2007. Carbon materials for supercapacitor application. Phys. Chem. Chem. Phys. 9, 1774–1785.
Guo, Y., Qi, J., Jiang, Y., Yang, S., Wang, Z., Xu, H., 2003. Performance of electrical double layer capacitors with porous carbons derived from rice husk. Mater. Chem. Phys. 80, 704–709.
Hulicova, D., Yamashita, J., Soneda, Y., Hatori, H., Kodama, M., 2005. Supercapacitors prepared from melamine-based carbon. Chem. Mater. 17, 1241–1247.
Ismanto, A.E., Wang, S., Soetaredjo, F.E., Ismadji, S., 2010. Preparation of capacitor's electrode from cassava peel waste. Bioresour. Technol. 101, 3534–3540.
Kim, Y.J., Lee, B.J., Suezaki, H., Chino, T., Abe, Y., Yanagiura, T., Park, K.C., Endo, M., 2006. Preparation and characterization of bamboo-based activated carbons as electrode materials for electric double layer capacitors. Carbon 44, 1592–1595.
Kinoshita, K., 1988. Carbon: Electrochemical and Physicochemical Properties. Wiley, New York.
Li, X., Xing, W., Zhuo, S., Zhou, J., Li, F., Qiao, S.Z., Lu, G.Q., 2011. Preparation of capacitor's electrode from sunflower seed shell. Bioresour. Technol. 102, 1118–1123.
Lillo-Ródenas, M.A., Cazorla-Amorós, D., Linares-Solano, A., 2003. Understanding chemical reactions between carbons and NaOH and KOH: an insight into the chemical activation mechanism. Carbon 41, 267–275.

Moreno-Castilla, C., Ferro-García, M.A., Joly, J.P., Bautista-Toledo, I., Carrasco-Marín, F., Rivera-Utrilla, J., 1995. Activated carbons surface modifications by nitric acid, hydrogen peroxide and ammonium peroxydisulfate treatments. Langmuir 11, 4386–4392.

Moreno-Castilla, C., Carrasco-Marín, F., Mueden, A., 1997. The creation of acid carbon surfaces by treatment with $(NH_4)_2S_2O_8$. Carbon 35, 1619–1626.

Moreno-Castilla, C., Carrasco-Marín, F., López-Ramón, M.V., Álvarez-Merino, M.A., 2001. Chemical and physical activation of olive-mill waste water to produce activated carbons. Carbon 39, 1415–1420.

Moreno-Castilla, C., Dawidziuk, M., Carrasco-Marín, F., Morallón, E., in press. Electrochemical performance of carbon gels with variable surface chemistry and physics. Carbon. <http://dx.doi.org/10.1016/j.carbon.2011.12.047>.

Pandolfo, A.G., Hollenkamp, A.F., 2006. Carbon properties and their role in supercapacitors. J. Power Sources 157, 11–27.

Pels, J.R., Kapteijn, F., Moulijn, J.A., Zhu, K., Thomas, K.M., 1995. Evolution of nitrogen functionalities in carbonaceous materials during pyrolysis. Carbon 33, 1641–1653.

Qu, D., Shi, H., 1998. Studies of activated carbons used in double-layer capacitors. J. Power Sources 74, 99–107.

Rodríguez-Reinoso, F., Linares-Solano, A., 1989. Microporous structure of activated carbons as revealed by adsorption methods. In: Thrower, P.A. (Ed.), Chemistry and Physics of Carbon, vol. 21. Marcel Dekker, New York, pp. 1–146.

Rufford, T.E., Hulicova-Jurcakova, D., Zhu, Z., Lu, G.Q., 2008. Nanoporous carbon electrode from waste coffee beans for high performance supercapacitors. Electrochem. Commun. 10, 1594–1597.

Rufford, T.E., Hulicova-Jurcakova, D., Khosla, K., Zhu, Z., Lu, G.Q., 2010. Microstructure and electrochemical double-layer capacitance of carbon electrodes prepared by zinc chloride activation of sugar cane bagasse. J. Power Sources 195, 912–918.

Seredych, M., Hulicova-Jurcakova, D., Gao, Q.L., Bandosz, T.J., 2008. Surface functional groups of carbons and the effects of their chemical character, density and accessibility to ions on electrochemical performance. Carbon 46, 1475–1488.

Subramanian, V., Luo, C., Stephan, A.M., Nahm, K.S., Thomas, S., Wei, B., 2007. Supercapacitors from activated carbon derived from banana fibers. J. Phys. Chem. C 111, 7527–7531.

Ubago-Pérez, R., Carrasco-Marín, F., Fairén-Jiménez, D., Moreno-Castilla, C., 2006. Granular and monolithic activated carbons from KOH-activation of olive stones. Micropor. Mesopor. Mater. 92, 64–70.

Villar-Rodil, S., Denoyel, R., Rouquerol, J., Martínez-Alonso, A., Tascón, J.M.D., 2002. Characterization of aramid based activated carbon fibres by adsorption and immersion techniques. Carbon 40, 1376–1380.

Wu, F.C., Tseng, R.L., Hu, C.C., Wang, C.C., 2004. Physical and electrochemical characterization of activated carbons prepared from firwoods for supercapacitors. J. Power Sources 138, 351–359.

Wu, F.C., Tseng, R.L., Hu, C.C., Wang, C.C., 2005. Effects of pore structure and electrolyte on the capacitive characteristics of steam- and KOH-activated carbons for supercapacitors. J. Power Sources 144, 302–309.

Zhang, L.L., Zhao, X.S., 2009. Carbon-based materials as supercapacitor electrodes. Chem. Soc. Rev. 38, 2520–2531.

Zhao, L., Fan, L.Z., Zhou, M.Q., Guan, H., Qiao, S., Antonietti, M., Titirici, M.M., 2010. Nitrogen-containing hydrothermal carbons with superior performance in supercapacitors. Adv. Mater. 22, 5202–5206.